Phase Coexistence of a Stockmayer Fluid in an Applied Field

Mark J. Stevens and Gary S. Grest

Corporate Research Science Laboratories, Exxon Research and Engineering Company, Annandale, NJ 08801

(February 8, 2008)

Abstract

We examine two aspects of Stockmayer fluids which consists of point dipoles that additionally interact via an attractive Lennard-Jones potential. We perform Monte Carlo simulations to examine the effect of an applied field on the liquid-gas phase coexistence and show that a magnetic fluid phase does exist in the absence of an applied field. As part of the search for the magnetic fluid phase, we perform Gibbs ensemble simulations to determine phase coexistence curves at large dipole moments, μ. The critical temperature is found to depend linearly on μ^2 for intermediate values of μ beyond the initial nonlinear behavior near $\mu = 0$ and less than the μ where no liquid-gas phase coexistence has been found. For phase coexistence in an applied field, the critical temperatures as a function of the applied field for two different μ are mapped onto a single curve. The critical densities hardly change as a function of applied field. We also verify that in an applied field the liquid droplets within the two phase coexistence region become elongated in the direction of the field.

I. INTRODUCTION

Dipolar fluids have a simple, but anisotropic, long-range pair potential which presents an interesting new set of problems for statistical physics. Manifestations of dipolar fluids include ferrofluids (FF), magnetorheological fluids (MR), electrorheological fluids (ER) and polar fluids [1–4]. These fluids have great technological promise and in some cases applications, as they possess the dual properties of being fluid and magnetic (electric). In most cases, an applied field is present. For the MR and ER fluids, an applied field is essential, since only induced dipoles exists.

Simulations of simple dipolar fluids have discovered several interesting phenomena. The fluid can become magnetized in the absence of an applied field at high densities [5,6]. For the simplest model of hard or soft sphere dipoles in zero field, no liquid-gas phase coexistence has been found in contrast to predictions of mean field theory [7–9]. In an applied field phase coexistence does occur for this system, yet it is not the usual gas-liquid or even isotropic-magnetic liquid phase coexistence [9]. Coexistence in the absence of an applied field does not occur in part because the only attractive interaction is the anisotropic dipolar interaction which tends to produces chains instead of droplets. Phase coexistence does occur in zero field if a sufficiently strong, short-range attractive interaction is added to the dipolar interaction [8].

One model that exhibits two phase coexistence in zero external field is the Stockmayer fluid (SF) [10,11]. This system consists of long-range dipoles that have an additional short-range Lennard-Jones (LJ) interaction. Since the LJ interaction alone is sufficient to produce a gas-liquid coexistence [12], it is clear that the Stockmayer fluid must also have a gas-liquid coexistence at least for small dipole moments. Recent simulations [10] have calculated the coexistence curves for several nonperturbative values of the dipolar moment, μ, in zero external magnetic field. For this reason the Stockmayer fluid is a good system to study the effects of an applied field on the gas-liquid phase coexistence.

One intriguing aspect of dipolar fluids is the existence of a magnetic fluid phase in the

absence of an applied field. For soft sphere dipoles, simulations have found a magnetic fluid phase [5,6] at high densities. Early simulations on the Stockmayer fluid for relatively small μ found negative pressures at these high densities [11]. Consequently, later studies of the ordering in the fluid preferred the hard or soft sphere dipolar system [5,6]. We now know that the negative pressures occur because of the two phase coexistence present in the Stockmayer fluid. Prior to this work, there have been no simulations to examine whether the magnetic liquid phase exists for a Stockmayer fluid at densities above the liquid coexistence curve. We report here results of simulations for the Stockmayer fluid that search for the magnetic liquid phase. The phase coexistence curves were calculated for larger values of μ where the magnetic liquid phase is more likely. Using these calculated coexistence curves we examined the regime above the liquid coexistence densities and find the magnetic liquid phase.

The Stockmayer fluid provides a simple model system for ferrofluids [13]. Recent work [8,9,14] has shown that a dipole with a purely repulsive core potential does not model some aspects of ferrofluids and that the presence of an additional attractive interaction is essential for phase coexistence. Experiments on hydrocarbon based ferrofluids have shown that phase coexistence depends strongly on the solvent [15,16]. For some solvents phase coexistence in the absence of an applied field does occur [16], while for others it does not [15]. Given that the same behavior occurs in simple dipolar systems as a function of the strength of the attractive part of the interaction, an examination of such systems is warranted.

In the next section, we describe the simulation methods employed. We also show that the variant of the Stockmayer potential used in Ref. [8] can be mapped to the standard Stockmayer potential. In section III, we present calculations of the coexistence curves for large μ and verify the mapping determined in section II. The existence of the magnetic fluid phase is demonstrated in section IV. In section V we examine the effect of an applied field on phase coexistence.

II. SIMULATION METHODS

The dipole-dipole interaction between particles i and j is

$$U_{dd}(\mathbf{r}_{ij}) = \frac{\mu^2}{r_{ij}^3}\left(\hat{\boldsymbol{\mu}}_i \cdot \hat{\boldsymbol{\mu}}_j - 3(\hat{\boldsymbol{\mu}}_i \cdot \hat{\mathbf{r}}_{ij})(\hat{\boldsymbol{\mu}}_j \cdot \hat{\mathbf{r}}_{ij})\right), \tag{1}$$

where $\boldsymbol{\mu}_i$ is the dipole moment of the ith particle, $\mathbf{r}_{ij}$ is the displacement vector between the two particles and a hat signifies a unit vector. There are three relevant parameters for the dipolar systems: the density, ρ, the dimensionless dipolar coupling strength given by the ratio, $\lambda = \mu^2/\sigma^3 T$, where σ is the particle diameter, and the dimensionless applied field, $\eta = \mu H/T$. The temperature may also be an independent variable depending on the nondipolar interactions. In any case, the dimensionless temperature is $\tau = 1/\lambda$.

In addition to the dipole interaction the Stockmayer fluid possesses a Lennard-Jones pair potential which models the van der Waals interactions in ferrofluids [1],

$$U_{LJ}(r_{ij}) = 4\varepsilon\left[\left(\frac{\sigma}{r_{ij}}\right)^{12} - \left(\frac{\sigma}{r_{ij}}\right)^{6}\right]. \tag{2}$$

The temperature and λ are now independent quantities. The LJ system with no dipole interaction ($\mu = 0$) has a critical point at $T_c^* = 1.316$ and $\rho_c^* = 0.304$ [17], where variables are given in reduced form: $T^* = T/\varepsilon$, $\rho^* = \rho\sigma^3$, $\mu^{*2} = \mu^2/\varepsilon\sigma^3$ and $H^* = H\sqrt{\sigma^3/\varepsilon}$. This critical point value is for a LJ cutoff equal to half the box length which is shifted slightly from the critical point of the LJ with no cutoff [18]. To maintain consistency we always use a cutoff equal to half the box length as was done in previous simulations for the Stockmayer fluid in zero field for several values of $\mu^{*2} \leq 6$ [10]; at $\mu^* = 2$, the critical point is $T_c^* = 2.09$ and $\rho_c^* = 0.289$ [10].

Recent simulations examined ostensibly a different system in which the strength of the attractive part of the LJ interaction was varied [8]. Specifically, they used the potential

$$U_{LJ6}(r_{ij}) = 4\varepsilon\left[\left(\frac{\sigma}{r_{ij}}\right)^{12} - \epsilon_6\left(\frac{\sigma}{r_{ij}}\right)^{6}\right], \tag{3}$$

where ϵ_6 is the constant used to vary the strength of the attractive interaction. We will refer to the system of dipoles with U_{LJ6} as the SF6 system. They found phase coexistence

for $\epsilon_6 \gtrsim 0.30$. For smaller values of ϵ_6, two phase coexistence was not detected by the Gibbs ensemble simulations and near the expected critical points chain formation was found instead. Thus, there seems to be a minimum amount of attraction necessary for a dipolar liquid phase to exist. This is consistent with the absence of phase coexistence for the soft sphere dipolar system, $\epsilon_6 = 0$ [9,14].

The significant feature of the interaction is not the absolute strength of the nondipolar attraction, but the relative strength in comparison with dipolar interaction. This is because the dipole interaction induces a condensed phase different from the LJ interaction, and consequently, the phase diagrams for LJ and strong dipolar (e.g. soft sphere dipoles) systems are different [9]. The dipolar interaction because of its orientation dependence prefers to aggregate particles in anisotropic chain structures instead of isotropic droplets like the LJ interaction prefers. That the relative strengths are the essential quantity is evident from that fact that U_{LJ6} can be mapped onto U_{LJ} [19]. Mapping

$$\sigma' = \sigma/\epsilon_6^{1/6}, \tag{4}$$

and

$$\varepsilon' = \varepsilon\epsilon_6^2 \tag{5}$$

converts the LJ6 parameters, σ and ε, into LJ parameters σ' and ε'. The density and temperature are mapped in the following manner

$$\rho' = \rho/\epsilon_6^{1/2}, \tag{6}$$

and

$$T' = T/\epsilon_6^2. \tag{7}$$

We can map the dipolar system, SF6, to SF by

$$\mu' = \mu/\epsilon_6^{3/4}. \tag{8}$$

Thus, reducing ϵ_6 as was done in Ref. [8] is equivalent to increasing the effective dipole moment. We confirm this mapping in section III. From the results of ref. [8], this mapping implies that for the Stockmayer fluid there is no phase coexistence for $\mu^* \gtrsim 5$.

Our simulations methods follow that of previous works on dipolar systems [5,6,10,20,21]. We performed simulations in zero field at $\mu^* = 2.5$, 3.0, 3.5 and 4.0. Simulations as a function of the applied field were performed at $\mu^* = 1$ and 2.5. The Ewald sum is used to evaluate the dipole interaction in periodic boundary conditions with the convergence parameter, $\alpha = 5.75$, and reciprocal vectors are summed to $10\pi/L$ where L is the length of the simulation cell. The Ewald sum contains a boundary term for the total potential energy

$$\frac{4\pi}{(2\mu_{BC}+1)L^3}\mathbf{M^2}, \tag{9}$$

where $\mathbf{M} = \sum_i \mu_i$ is the magnetization. We use $\mu_{BC} = \infty$ making the above term zero. This allows the uniformly magnetized state to occur. A value of $\mu_{BC} = 1$ will lead to magnetic domains because this condition prevents the system from having a net magnetization [6]. This form of the Ewald sum treats a periodic lattice enclosed in a large sphere or cube [22]. These boundary conditions are consistent with experiments performed between parallel plates. As mentioned above, the LJ cutoff was set at half the box length and the usual long range corrections were employed [23].

In recent density functional calculations [24], it was found that the phase coexistence depends on shape of the system volume. In these calculations, the system was taken as an ellipsoid of revolution with axis of revolution k times the other two axes. The magnetic fluid phase is favored for large k. Simulations with the Ewald sum usually treat a cubic, or equivalently spherical, system [22]. The cube has sidelength, $S \gg L$, where L is the simulation box length. The simulation is generally viewed as modeling a microscopic piece of the bulk system. For example, with respect to ferrofluids which are often experimentally studied confined between parallel plates, the simulation models a cube within the middle of the system. Ideally, one wants to choose μ_{BC} equal to the permeability of the bulk system, μ_{bulk}, but that requires *a priori* knowledge which one does not have. Recent simulations

have shown that the difference between using $\mu_{BC} = \infty$ and $\mu_{BC} = \mu_{bulk}$ is small as long as μ_{bulk} is large [6].

To examine the liquid structure we performed constant volume canonical ensemble simulations with $N = 256$ particles. These simulations ran for a least 10^5 MC cycles with each cycle comprised of an attempt to translate and rotate each particle. The particle step size was chosen to achieve about 50% acceptance. The rotation step was usually set so that the component of the new moment in the direction of the old moment was at most 0.2. This was done for most cases since the acceptance rate could not be lowered to 50%. The rotation step size was lowered below 0.2, when that would yield a 50% acceptance.

Gibbs ensemble simulations were performed to determine the coexistence curves and critical points [25,26]. Below the critical temperature the Gibbs ensemble directly gives the two coexistence densities at a given temperature. For most of the Gibbs simulations, $N = 512$. Some simulations were performed with $N = 1024$ to test the N dependence. The Gibbs simulations required at least 10^4 cycles. The larger μ^* simulations required runs 2-5 times longer. Long runs were also performed for temperatures near T_c. Each cycle included an attempt to move each particle once, 100 attempts to change the cell volume and 500 attempts to exchange particles between the two cells. Only a small percentage of exchanges is accepted in these Gibbs simulations. Thus, an extremely large number of attempts is needed to gather reasonable statistics. For our simulations at least 10,000 accepted exchanges occured in 10,000 cycles. We have verified that both the pressures and the chemical potentials are the same in the two cells. The pressure is calculated from the virial expression and the chemical potential is calculated from the overlap of the particle insertion and extraction energy distributions [27].

Our simulations in the Gibbs ensemble were performed with H^* ranging from 0 to 5. The critical temperature, T_c, and density, ρ_c, were determined by fitting the calculated coexistence curves using the law of rectilinear diameters and the usual scaling law for the density with exponent $\beta = 0.32$ [28].

We characterize the system structure through the order parameter, P_1, defined as

$$P_1 = \frac{1}{N}\sum_{i=1}^{N} \hat{\boldsymbol{\mu}}_i \cdot \hat{\mathbf{d}} = \frac{1}{\mu N}\mathbf{M}\cdot\hat{\mathbf{d}}, \tag{10}$$

where $\hat{\mathbf{d}}$ is the director and $\mathbf{M}$ is the total magnetization of the system. For a completely magnetized system, $P_1 = 1$.

III. PHASE COEXISTENCE AT LARGE μ^*

In order to examine the possibility of a magnetic fluid phase, we performed simulations at larger μ^* than previous works [10]. Using Gibbs ensemble simulations we determined the coexistence curves for $\mu^* = 2.5$, 3.0, 3.5 and 4.0. The critical points are given in Tables II. We then performed constant volume canonical ensemble simulations at densities above the liquid coexistence densities looking for a magnetic fluid phase. Before discussing the magnetic fluid phase, we discuss the μ^* dependence of the critical point.

We plot T_c^* as a function of μ^{*2} in Fig. 1(a). The open squares are from previous simulations [10], our data are the open circles and the solid circles are the mapped data of Ref. [8]. For $\mu^{*2} \geq 2$ a linear fit to T_c^* with slope 0.254 and intercept 1.06 fits the data well. This fit must end near $\mu^{*2} \simeq 24$ where no coexistence was found [8]. The parameterization given by van Leeuwen [10](c) fits the T data except at large μ^{*2}. Clearly, the data is consistent with the mapping given in Eqs. 4-8. For small μ^*, the dipole interaction is effectively a r^{-6} van der Waals attraction [19]. This increases the total attraction and consequently, T_c is raised and ρ_c is lowered as seen in Fig. 1. For large μ^*, this basic trend continues and T_c has a simple dependence.

Similar results are found for ρ_c in Fig. 1(b). There is more uncertainty in this data, but a least squares fit calculated as above gives the general decreasing trend with increasing μ^*. Here, the parameterization of van Leeuwen only works for the original data fitted.

As noted earlier, we can also define the dimensionless (dipolar) temperature, τ. The critical value, τ_c, is more relevant to determining the dipolar structure. In Fig. 2 we plot τ_c as a function of μ^{*2}. The solid line is the equation

$$\tau_c = 0.254 + \frac{1.06}{\mu^{*2}} \tag{11}$$

derived from the linear fit in Fig. 1. The equation suggests an apparent saturation of τ_c to about 0.25. However, the largest value of μ^{*2} for which phase coexistence has been found ($\mu^{*2} = 24.34$ from $\epsilon_6 = 0.30$ [8]) has $\tau_c = 0.30$. Beyond $\mu^{*2} \simeq 24$ Eq. 11 does not hold and the lowest critical dimensionless temperature is $\tau_c = 0.30$. At higher μ^* the fluid structure in the vicinity of the τ_c from Eq. 11 exhibits chain formation [8]. This change in fluid structure precludes liquid-gas phase coexistence.

IV. MAGNETIC FLUID PHASE

We now address the question of the existence of a magnetic fluid phase in the absence of an applied field in the Stockmayer fluid. A magnetic fluid phase has already been found in the soft sphere dipolar system for $\lambda \gtrsim 4$ [5,6,9,14] at high densities. To determine if the magnetic fluid phase exists for the Stockmayer fluid, we examine densities larger than the liquid coexistence densities, ρ_ℓ. We use the coexistence curves calculated in the last section to determine the density region of interest. The coexistence curves for larger μ^* were calculated in the last section because a sufficiently large $\lambda \gtrsim 1$ is necessary for existence of the magnetic fluid phase as found for the soft sphere system. For $\lambda \lesssim 1$, thermal interactions dominate and there is no magnetic fluid phase.

We find that for the Stockmayer fluid the structure of liquid coexisting phase in our Gibbs simulations is isotropic. It is possible for the coexisting liquid phase to be magnetically ordered [24,29–31], but that is more likely to occur in the case of a liquid-liquid coexistence, where one liquid phase is isotropic and the other is magnetic. In the canonical ensemble simulations at $T << T_c$, we do find some ordering, but this is most likely a finite size effect. Figure 3 shows the Gibbs ensemble data and the fit to the coexistence curve for $\mu^* = 2.5$. Obviously, far from T_c^*, the coexistence curve will probably not follow the simple fit function used, but we are only concerned about having a guide to choose where to perform simulations. The squares show the ρ^* and T^* at which simulations were performed in this

case. A solid square denotes a negative pressure and is within the coexistence region as expected. Similar simulations were performed for $\mu^* = 3.0$ and 3.5. The results are given in Table III.

At T_c, the values of $\lambda \equiv \lambda_c$ are too low for the magnetic fluid phase based on our experience with the soft sphere dipolar fluid. For soft sphere dipoles, we found that for $\lambda = 4$, the magnetic fluid phase occurs close to $\rho^* = 1.0$ [14]. For the Stockmayer fluid, we find for $\mu^* = 2.5$, $\lambda_c = 2.38$. Thus, any magnetic fluid behavior, if it occurs at all, will occur at T much lower than T_c. The situation does not improve much with increasing μ^* since the value of $\tau_c = 1/\lambda_c$ (see Fig. 2) saturates for large μ^*. Thus, even for $\mu^* = 4.0$, λ_c is only 3.17. To have a chance of finding a magnetic fluid phase, T must be much lower than T_c and of course, $\rho > \rho_\ell$. As T decreases, ρ_ℓ increases and we will encounter the solid phase certainly by $\rho^* = \sqrt{2}$, the close packed density. For hard sphere dipoles, the liquid-solid transition for $\mu^* = 2.5$ occurs at $\rho^* \simeq 1.0$ [32]. Thus, the existence of a magnetic fluid phase depends on part on where the triple point temperature and density are. If the triple point temperature is sufficiently low, a magnetic fluid phase may exist in the region above the triple point.

Calculated phase diagrams [24,30] have shown the critical point for the isotropic-magnetic coexistence to be at a higher temperature than the gas-liquid T_c even for $\mu^* = 2$. This is inconsistent with our simulation results, although the density functional calculations [24] are primarily for ellipsiodal geometries, not the spherical geometries used in the simulations. The anisotropy of the ellipsoid promotes the magnetic fluid phase. For spherical geometry, the results are consistent with our results. Our simulations also show that the value of λ near T_c is too small for ordering to occur. Table III shows that P_1 is small for $\mu^* = 2.5$ at $\rho^* = 0.8$ and $T^* = 2.5$ which is slightly below T_c^*. Furthermore, as T^* decreases at this density, it is not until $T^* = 1.5$ that $P_1 \geq 0.5$, and at $T^* = 2.0$ $P_1 < 1/2$ for $\rho^* < 1.0$. Thus, for the spherical geometry, the simulations show that the gas-liquid T_c is too high for a magnetic fluid phase to exist above it.

For $\mu^* = 2.5$, Table III shows that for $T^* \lesssim 1.5$, $P_1 > 0.5$. We take the magnetic liquid transition density to be where $P_1 = 0.50$. There will be of course finite size effects [33] which

tend with increasing N to lower P_1 below the transition and increase it above the transition. Here, we are mainly interested in the existence of the transition as opposed to pinning down the transition point which would require simulations with much larger values of N. For $\lambda = 4.19$, we find the transition at $\rho^* \simeq 0.90$. There is the possibility that the system is a supercooled liquid at this density. However, since the transition for hard sphere dipoles at $\lambda = 6.25$ is at $\rho^* \simeq 1.0$, we are most likely below the liquid-solid transition. Furthermore, we have found that the fcc crystal phase melts at $\rho^* = 1.0$, although the fcc crystal is most likely not the solid phase ground state [32]. In general, Table III shows that for $\lambda \gtrsim 4.0$ and $\rho^* \gtrsim 0.90$, $P_1 \geq 0.50$ and a magnetic liquid regime exists.

V. PHASE COEXISTENCE IN AN APPLIED FIELD

Phase coexistence in an applied field was studied at two dipole moments, $\mu^* = 1.0$ and 2.5. We chose $\mu^* = 1$ since at $T_c(H = 0)$, $\lambda = 0.71$ so that the thermal and LJ interactions are about of equal strength. For $\mu^* = 2.5$, $\lambda = 2.38$ at $T_c(H = 0)$ and the dipole interactions are significantly larger than the LJ interactions. This is especially true near T_c. One might expect that the results for the two dipoles strongly differ, but we find that much of the results can be described in terms of dimensionless quantities that remove the μ^* dependence.

For $\mu^* = 1$ and large H^*, we encountered some difficulties in obtaining accurate values of the coexisting densities close to the critical point. This is a problem that has been observed before [25]. The free energy surface becomes rather flat and the simulation can become trapped away from the two minima. One might expect the problem to be worse for $\mu^* = 2.5$, but we found this not to be the case.

Figure 4 shows the phase coexistence curves for $\mu^* = 1$ and $\mu^* = 2.5$ at selected fields. As H increases, the dipoles become progessively aligned with the field direction. The dipolar interaction between pairs of particles is then stronger and the dipole moments are more correlated. The critical temperature increases with field due to the stronger dipolar interactions as is found in the absence of an applied field. In contrast to the varying T_c, the

critical density changes at most only slightly. For $\mu^* = 1.0$ the shape of the coexistence curve changes slightly as can be seen by the fact that the midpoint line becomes almost vertical. However, we can still fit the curves with $\beta = 0.32$ and the $\mu^* = 2.5$ midpoint lines maintain a negative slope. Because the midpoint line was more vertical for $\mu^* = 1$ than $\mu^* = 2.5$, more data was needed near T_c which tended to encounter the convergence problem mentioned above.

The field dependence of the critical temperature can be simplified by examining the critical temperature at H, $T_c(H)$, relative to the zero field critical temperature, $T_c(0)$ in terms of the ratio

$$T_c^H = \frac{T_c(H)}{T_c(0)}. \tag{12}$$

A collapse of the data (Fig. 5) for our two dipole moments is obtained when we plot T_c^H versus the dimensionless field using T_c^H as the temperature,

$$\eta_H \equiv \frac{\mu H}{k_B T_c^H}. \tag{13}$$

We have drawn a least squares fit to the data excluding the $H = 0$ point which fits the data within the uncertainty. Near $H = 0$ there must be some nonlinear behavior. At large H, i.e. beyond the saturation field, a μ dependence is expected because saturation is μ dependent. We have not reached the saturation H in our simulations. In order to determine T_c for the infinite field, we performed Gibbs ensemble simulations with the dipole moments fixed in the z-direction. For this case, we find $T_c^* = 3.64$ for $\mu^* = 2.5$. This yield $T_c^H = 1.38$ which from the fit occurs for $\eta_H = 20.5$ which is beyond the range we have studied. Thus, for the range of H we studied, we see no effects of field saturation.

We can also get an idea of how near the systems are to saturation by calculating the magnetization, M, or equivalently, P_1. In Tables IV and V we list the values of the order parameter, P_1. We want to calculate M at the critical point. The magnetization in the gas phase is basically constant as the dipoles only interact weakly. The interaction energy between a dipole pair will be $k_B T$ at a separation of $r = \lambda^{1/3}\sigma$. For $\rho^* \simeq 0.30$, the average

separation is $a = \rho^{-1/3} \simeq 1.5\sigma$. We are working in the range of $\lambda < 4$, which gives $r = 1.6\sigma$. Thus, the dipolar interaction energies are at most equal to $k_B T$. We take $M_c \equiv M(T_c)$ to be the value of M for the gas phase. In Fig. 6 we plot $M/\mu N$ for the two cases. Neither case has reached saturation, as we expected since there is no μ dependence in our T_c^H.

One of the important question concerning dipolar fluids (FF, MR, and ER) presently under consideration [2,3,16,34–36] is the shape of the liquid coexisting phase. We can only examine the structure at the particle level and are mainly concerned with confirming the basic effect of elongation of a liquid droplet in the applied field. We have performed a constant volume canonical ensemble simulation for $\mu^* = 2$ at $\rho^* = 0.01$, $T^* = 1.0$ and $H^* = 0$ and 1.0. In Fig. 7 we show projection plots for the two different H^*. In the absence of a field, the droplets are spherical on average as expected, and in the presence of a field the droplets become extended along the field direction (z in Figure) and in this case two of the droplets at $H^* = 0$ coalesced into one. Thus, we find the two main effects of an applied field on liquid droplets: elongation in the field direction and coalescence [37,38].

VI. CONCLUSION

The results of the the present simulations give a better understanding of the phase diagram of the Stockmayer fluid in both zero or nonzero fields. The mapping of the SF6 system onto the SF system shows that dipole interaction strength in comparison with the LJ interaction strength is the determining quantity for the occurance of phase coexistence. The mapping is particularly useful as discussed below when comparing with experimental systems as discussed below. The μ dependence of the critical point is rather simple for most of the range over which SF phase coexistence occurs. In this range, the temperature, T_c^* depends linearly on μ^2. Linear behavior is also true for ρ_c, although there is more uncertainty here. The magnetic fluid phase does appear at high densities for sufficently large μ. At least for the spherical geometry, the tricritical temperature appears to be below T_c. In an applied fields, a μ-independent scaling can be obtained at least for a broad range of fields for the

critical temperature as a function of applied field when the temperature is scaled by the zero field T_c.

One of the important conclusions of previous works [9,14] is that the hard or soft sphere dipolar systems were insufficient as models for ferrofluids (and most likely MR and ER fluids). Some added central force attraction is required such as found in the SF or SF6 potentials. Dipole moments in terms of λ are about 1, although ferrofluids possess a large polydispersity [1]. However, the residual strength of an attractive interaction such as van der Waals is unknown. Thus, the value of ϵ_6 must be determined from some experimental data. If phase coexistence occurs in zero field, one way of determing ϵ_6 is to map the value of T_c for $H = 0$, and the given value of μ onto the plot of T_c versus ϵ_6. In the cases where no phase coexistence occurs at $H = 0$, one must determine ϵ_6 from the value of T_c at $H > 0$. The linear relationships between T_c or ρ_c and μ^2 simplify this procedure somewhat. In some of the experiments [15] phase coexistence curves are not fully measured, but slices in the H-ρ plane at fixed T are measured. To compare with these experiments requires calculation of coexistence curves not only at several H, but also several T and ϵ_6 in order to determine the correct ϵ_6 and the make the correct slices.

The structure at the particle level in ferrofluids has not been resolved experimentally. Simulations naturally offer a means to examine this structure. The structure of the columnar objects [1,39] that form in ferrofluids is an open question. In the simulations of soft sphere dipoles, chains form consisting of connected single particles as in a polymer [9,14]. These chains do not aggregate to form the columnar structures as has been observed experimentally. In contrast, we find in the simulations of the Stockmayer fluid that the polymeric chains do not form. In an applied field, the zero field droplets distort becoming elongated in the field direction. Droplets are also seen to coalesce. This suggests that in ferrofluids that the columns are formed by initial formation of liquid droplets that are distorted into an elliptical shape and coalesce in an applied field to form columns spanning the experimental cell.

REFERENCES

[1] R. Rosensweig, *Ferrohydrodynamics* (Cambridge University Press, Cambridge, 1985).

[2] T. Halsey, Science **258**, 761 (1992).

[3] T. Halsey and J. Martin, Sci. Am. **269**, 58 (1993).

[4] M. van Leeuwen, Fluid Phase Equilibria **99**, 1 (1994).

[5] D. Wei and G. Patey, Phys. Rev. Lett. **68**, 2043 (1992).

[6] D. Wei and G. Patey, Phys. Rev. **A46**, 7783 (1992).

[7] J.-M. Caillol, J. Chem. Phys. **98**, 9835 (1993).

[8] M. van Leeuwen and B. Smit, Phys. Rev. Lett. **71**, 3991 (1993).

[9] M. J. Stevens and G. S. Grest, Phys. Rev. Lett. **72**, 3686 (1994).

[10] B. Smit, C. Williams, and E. Hendriks, Mol. Phys. **68**, 765 (1989); M. van Leeuwen, B. Smit, and E. Hendriks, Mol. Phys. **78**, 271 (1993); M. van Leeuwen, Mol. Phys. **82**, 383 (1994).

[11] E. L. Pollock and B. J. Alder, Physica **102A**, 1 (1980).

[12] J.-P. Hansen and I. McDonald, *Theory of Simple Liquids* (Academic Press, London, 1990).

[13] V. Russier and M. Douzi, J. Coll. Inter. Sci. **162**, 356 (1994).

[14] M. J. Stevens and G. S. Grest (unpublished).

[15] R. Rosensweig and J. Popplewell, in *Electromagnetic Forces and Applications* (Elsevier Science Publishers, New York, 1992), p. 83.

[16] H. Wang *et al.*, Phys. Rev. Lett. **72**, 1929 (1994).

[17] B. Smit, Ph.D. thesis, Rijksuniversiteit Utrecht, The Netherlands, 1990.

[18] J. Nicolas, K. Gubbins, W. Streett, and D. Tildesley, Mol. Phys. **37**, 1429 (1979).

[19] G. Stell, J. C. Rasaiah, and H. Narang, Mol. Phys. **23**, 393 (1972).

[20] P. Kusalik, J. Chem. Phys. **93**, 3520 (1990).

[21] P. Kusalik, Mol. Phys. **81**, 199 (1994).

[22] S. W. de Leeuw, J. W. Perram, and E. R. Smith, Proc. R. Soc. Lond. A **373**, 27 (1980).

[23] M. Allen and D. Tildesley, *Computer Simulation of Liquids* (Clarendon Press, Oxford, 1987).

[24] B. Groh and S. Dietrich, Phys. Rev. Lett. **72**, 2422 (1994); Phys. Rev. E50, 3814 (1994).

[25] B. Smit, in *Computer Simulation in Chemical Physics* (Kluwer Academic Publishers, Dordrecht, 1993), pp. 173–209.

[26] A. Panagiotopoulos, Mol. Sim. **9**, 1 (1992).

[27] J. Powles, W. Evans, and N. Quirke, Mol. Phys. **46**, 1347 (1982).

[28] B. Smit and C. Williams, J. Phys. Condens. Matter **2**, 4281 (1990).

[29] A. O. Tsebers, Magnetohydrodynamics **18**, 137 (1982).

[30] H. Zhang and M. Widom, Phys. Rev. **E49**, 3591 (1994).

[31] K. Sano and M. Doi, J. Phys. Soc. Jpn. **52**, 2810 (1983).

[32] J. Weis and D. Levesque, Phys. Rev. **E48**, 3728 (1993).

[33] K. Binder and D. Heermann, *Monte Carlo Simulation in Statistical Physics* (Springer Verlag, Berlin, 1988).

[34] Y. Grasselli, G. Bossis, and E. Lemaire, J. Phys. II France **4**, 253 (1994).

[35] M. Fermigier and A. Gast, J. Coll. Int. Sci. **154**, 522 (1992).

[36] J.-C. Bacri, D. Salin, and R. Massart, J. Physique Lett. **43**, 179 (1982).

[37] J. Liu, T. Mou, and G. A. Flores (unpublished).

[38] J. Liu, E. Lawrence, M. Ivey, and G. A. Flores (unpublished).

[39] D. Krueger, IEEE Trans. Magn. **16**, 251 (1980).

TABLES

TABLE I. Critical points.

μ^*	H^*	T_c^*	ρ_c^*
2.5	0.0	2.63(1)	0.29(1)
3.0	0.0	3.35(1)	0.25(1)
3.5	0.0	4.20(1)	0.24(1)
4.0	0.0	5.07(5)	0.24(1)
1.0[a]	0.0	1.41(1)	0.30(1)
1.0	1.0	1.44(1)	0.32(1)
1.0	2.0	1.49(1)	0.33(1)
1.0	3.0	1.51(1)	0.32(1)
2.5	0.5	2.71(1)	0.285(1)
2.5	1.0	2.78(1)	0.285(1)
2.5	2.0	2.89(1)	0.302(1)
2.5	5.0	3.15(1)	0.278(1)
2.5	∞	3.64(1)	0.303(1)

[a]Data from Ref. [8].

TABLE II. Phase coexistence data for $\mu^* = 3.0$, 3.5 and 4.0

T^*	μ^*	ρ_g^*	P_g^*	ρ_ℓ^*	P_ℓ^*
2.70	3.0	0.011(1)	0.021(1)	0.68(1)	0.01(5)
2.85	3.0	0.020(2)	0.036(3)	0.63(2)	0.02(5)
2.95	3.0	0.033(5)	0.053(3)	0.59(2)	0.05(2)
3.00	3.0	0.060(9)	0.057(5)	0.57(2)	0.05(6)
3.10	3.0	0.060(8)	0.077(1)	0.57(2)	0.09(6)
3.20	3.0	0.072(9)	0.099(5)	0.46(3)	0.09(1)
3.25	3.0	0.086(14)	0.099(2)	0.43(4)	0.11(1)
3.30	3.0	0.13(1)	0.124(4)	0.39(2)	0.12(1)
3.35	3.0	0.21(2)	0.148(5)	0.30(2)	0.14(2)
3.50	3.5	0.011(1)	0.025(2)	0.64(2)	0.03(9)
3.70	3.5	0.017(1)	0.043(2)	0.58(2)	0.03(3)
3.80	3.5	0.031(8)	0.046(6)	0.54(2)	0.03(2)
3.90	3.5	0.053(6)	0.070(6)	0.50(4)	0.06(3)
4.00	3.5	0.06(1)	0.084(4)	0.46(2)	0.09(3)
4.05	3.5	0.065(5)	0.091(9)	0.45(2)	0.10(2)
4.10	3.5	0.08(2)	0.101(4)	0.41(4)	0.12(2)
4.15	3.5	0.10(2)	0.111(4)	0.39(1)	0.11(3)
4.70	4.0	0.03(6)	0.04(5)	0.48(8)	0.01(4)
4.80	4.0	0.05(2)	0.07(2)	0.53(2)	0.10(3)
4.90	4.0	0.05(1)	0.072(4)	0.50(2)	0.07(4)
4.95	4.0	0.07(1)	0.09(1)	0.44(2)	0.08(3)
5.00	4.0	0.06(1)	0.08(1)	0.41(2)	0.07(3)
5.02	4.0	0.14(2)	0.08(5)	0.41(4)	0.09(2)

TABLE III. Data for dense liquid phase for $N = 256$.

μ^*	λ_B	T^*	ρ^*	P^*	P_1
2.5	2.50	2.5	0.80	2.83(3)	0.08(1)
2.5	3.12	2.0	0.75	0.33(1)	0.09(1)
2.5	3.12	2.0	0.80	0.98(4)	0.11(4)
2.5	3.12	2.0	0.85	1.97(3)	0.13(3)
2.5	3.12	2.0	0.95	5.21(2)	0.21(3)
2.5	4.16	1.5	0.80	-0.93(5)	0.24(2)
2.5	4.16	1.5	0.85	-0.41(4)	0.36(9)
2.5	4.16	1.5	0.90	0.36(4)	0.51(2)
2.5	4.16	1.5	0.95	1.57(7)	0.62(1)
2.5	4.16	1.5	1.00	3.26(5)	0.69(2)
3.0	4.09	2.2	0.80	-0.35(4)	0.17(10)
3.0	4.09	2.2	0.90	1.74(7)	0.33(5)
3.0	4.50	2.0	0.90	0.60(15)	0.55(6)
3.0	4.50	2.00	1.00	3.42(9)	0.71(1)
3.5	4.08	3.0	0.80	0.58(5)	0.20(4)
3.5	4.08	3.00	0.90	2.70(7)	0.29(5)
3.5	4.45	2.75	0.80	0.00(14)	0.22(8)
3.5	4.45	2.75	0.90	1.62(12)	0.41(10)
3.5	4.90	2.50	0.90	0.37(17)	0.64(2)
3.5	4.90	2.50	1.00	2.98(7)	0.76(2)

TABLE IV. Phase coexistence data in fields for $\mu^* = 1.0$

T^*	H^*	ρ_g^*	P_g^*	$P_1^{(g)}$	ρ_ℓ^*	P_ℓ^*	$P_1^{(\ell)}$
1.10	1.0	0.025(2)	0.023(2)	0.24(4)	0.724(5)	0.024(7)	0.477(3)
1.20	1.0	0.047(3)	0.043(3)	0.21(2)	0.669(5)	0.046(7)	0.43(1)
1.30	1.0	0.080(5)	0.071(3)	0.22(5)	0.602(5)	0.072(6)	0.366(7)
1.35	1.0	0.113(7)	0.092(3)	0.21(7)	0.554(7)	0.083(8)	0.341(7)
1.37	1.0	0.122(9)	0.098(4)	0.22(2)	0.54(1)	0.09(2)	0.31(1)
1.40	1.0	0.15(1)	0.11(3)	0.22(2)	0.48(2)	0.100(7)	0.30(3)
1.30	2.0	0.077(6)	0.069(2)	0.46(1)	0.629(6)	0.067(7)	0.60(1)
1.35	2.0	0.090(5)	0.079(4)	0.45(2)	0.590(4)	0.08(2)	0.57(1)
1.40	2.0	0.109(5)	0.096(2)	0.44(1)	0.544(8)	0.094(9)	0.55(1)
1.44	2.0	0.157(9)	0.117(2)	0.45(2)	0.50(1)	0.118(6)	0.53(2)
1.46	2.0	0.186(8)	0.129(3)	0.45(1)	0.49(2)	0.132(7)	0.52(1)
1.48	2.0	0.21(3)	0.138(5)	0.46(1)	0.45(2)	0.141(8)	0.51(1)
1.30	3.0	0.056(8)	0.055(5)	0.60(1)	0.646(3)	0.05(1)	0.70(1)
1.35	3.0	0.078(4)	0.072(2)	0.60(1)	0.614(8)	0.06(1)	0.69(1)
1.40	3.0	0.099(5)	0.088(2)	0.58(1)	0.575(17)	0.08(2)	0.67(1)
1.45	3.0	0.132(11)	0.108(6)	0.60(1)	0.529(6)	0.104(6)	0.65(1)
1.45	3.0	0.129(11)	0.108(6)	0.58(1)	0.518(16)	0.103(9)	0.65(1)
1.47	3.0	0.157(6)	0.120(1)	0.58(1)	0.51(2)	0.12(2)	0.65(1)

TABLE V. Phase coexistence data in fields for $\mu^* = 2.5$

T^*	H^*	ρ_g^*	P_g^*	$P_1^{(g)}$	ρ_ℓ^*	P_ℓ^*	$P_1^{(\ell)}$
2.30	0.5	0.03(1)	0.045(4)	0.20(1)	0.66(1)	0.05(1)	0.53(2)
2.40	0.5	0.04(1)	0.06(1)	0.16(1)	0.62(1)	0.07(2)	0.50(2)
2.50	0.5	0.09(1)	0.092(3)	0.21(2)	0.56(1)	0.09(3)	0.44(3)
2.60	0.5	0.16(3)	0.118(6)	0.23(2)	0.49(2)	0.12(1)	0.40(1)
2.65	0.5	0.14(1)	0.14(1)	0.20(5)	0.44(4)	0.14(2)	0.36(1)
2.70	0.5	0.21(5)	0.16(1)	0.22(6)	0.38(5)	0.16(3)	0.33(1)
2.40	1.0	0.030(5)	0.048(6)	0.34(2)	0.66(1)	0.05(3)	0.68(1)
2.50	1.0	0.046(5)	0.069(4)	0.33(4)	0.61(1)	0.07(2)	0.64(1)
2.65	1.0	0.09(2)	0.109(4)	0.38(4)	0.51(2)	0.10(4)	0.59(1)
2.70	1.0	0.11(2)	0.127(8)	0.39(1)	0.49(3)	0.136(3)	0.57(1)
2.72	1.0	0.13(2)	0.133(7)	0.40(2)	0.47(1)	0.13(1)	0.56(2)
2.73	1.0	0.12(2)	0.133(10)	0.39(4)	0.44(3)	0.13(1)	0.54(2)
2.74	1.0	0.15(2)	0.137(7)	0.43(4)	0.45(1)	0.14(1)	0.55(1)
2.40	2.0	0.019(1)	0.034(4)	0.61(4)	0.702(3)	0.03(5)	0.80(1)
2.50	2.0	0.028(3)	0.047(3)	0.59(3)	0.664(5)	0.06(3)	0.78(1)
2.60	2.0	0.040(6)	0.066(6)	0.59(3)	0.623(6)	0.07(6)	0.77(1)
2.70	2.0	0.069(11)	0.093(6)	0.60(2)	0.585(13)	0.10(1)	0.75(1)
2.80	2.0	0.10(2)	0.118(10)	0.60(2)	0.516(6)	0.13(1)	0.72(1)
2.85	2.0	0.13(2)	0.136(3)	0.61(2)	0.50(2)	0.14(1)	0.72(1)
2.80	5.0	0.043(8)	0.070(5)	0.82(1)	0.609(6)	0.063(5)	0.86(1)
2.90	5.0	0.058(6)	0.091(6)	0.80(1)	0.579(8)	0.09(2)	0.86(1)
3.00	5.0	0.10(2)	0.118(7)	0.80(1)	0.54(2)	0.12(2)	0.85(1)
3.05	5.0	0.09(1)	0.13(1)	0.80(1)	0.48(1)	0.122(8)	0.86(1)
3.08	5.0	0.12(2)	0.14(1)	0.80(1)	0.46(3)	0.14(3)	0.83(1)
3.10	5.0	0.12(2)	0.14(2)	0.80(1)	0.44(2)	0.14(1)	0.83(1)

FIGURES

FIG. 1. In (a) the critical temperature, T_c^*, as a function of the dipole moment squared, μ^{*2}, and in (b) the critical density ρ_c^* is plotted. The open points are from previous works [10] and the solid points are from this work. The solid lines are a least squares fit to the nonzero μ^* data. The dotted lines are the parameterizations given in ref. [10](c). The uncertainty in T_c^* is about ± 0.01 for all data which is smaller than the points.

FIG. 2. The dimensionless temperature, τ_c, is plotted versus μ^{*2} with the same point types as in Fig. 1. The solid line is obtained from the least squares fit in Fig. 1.

FIG. 3. The coexistence curve calculated in the Gibbs ensemble simulation in the absence of an applied field at $\mu^* = 2.5$ is plotted. The open circles are the coexisting density points found in the simulations. The solid circle represents the critical point calculated along with the fitting curve as described in the text. The square represents points where canonical simulations were performed to determine the existence of the magnetic fluid phase (see also Table III).

FIG. 4. The coexistence curves within an applied field are plotted (a) for $\mu^* = 1$ at $H^* = 0$, 1, 2 and 3, and (b) for $\mu^* = 2.5$ at $H^* = 0$, 0.5, 1.0, 2.0 and 5.0.

FIG. 5. The critical temperature for systems exhibits some scaling when plotted versus the dimensionless field. In order for the data of the two μ^* to be on the same curve, we scale $T_c^*(H)$ by the zero field T_c^*. This is also done in the dimensionless field. The solid line is a least squares fit to the nonzero field data.

FIG. 6. The magnetization per particle versus the applied field for $\mu^* = 1$ (triangles) and $\mu^* = 2.5$ (squares).

FIG. 7. Projection plots for (a) $H^* = 0$ and (b) $H^* = 1.0$ for $\mu^* = 2$ at $\rho^* = 0.1$ and $T^* = 1$ show the effect of an applied field on the liquid droplet shape in the coexistence region. The field is parallel to the z-direction.

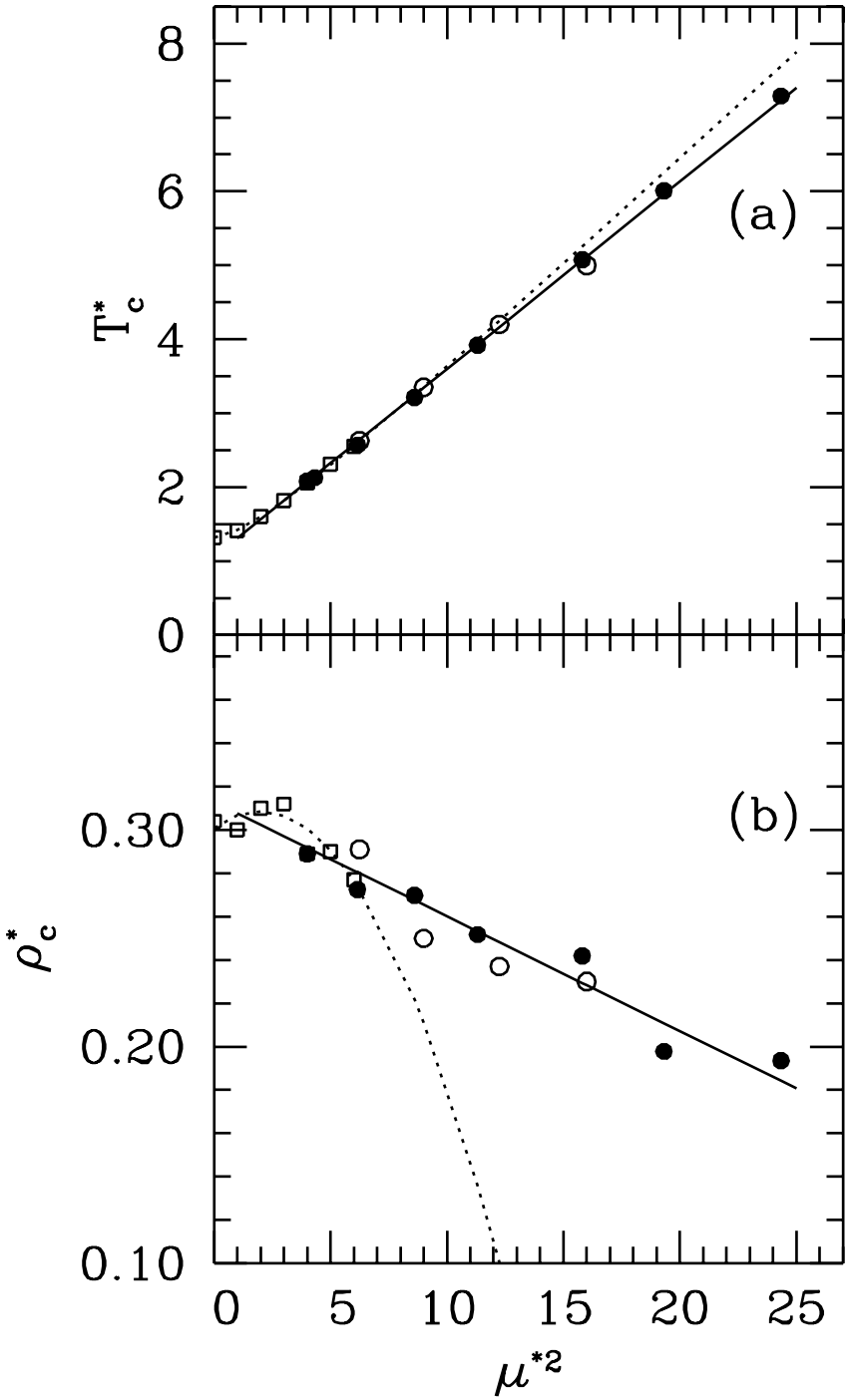

Figure 1

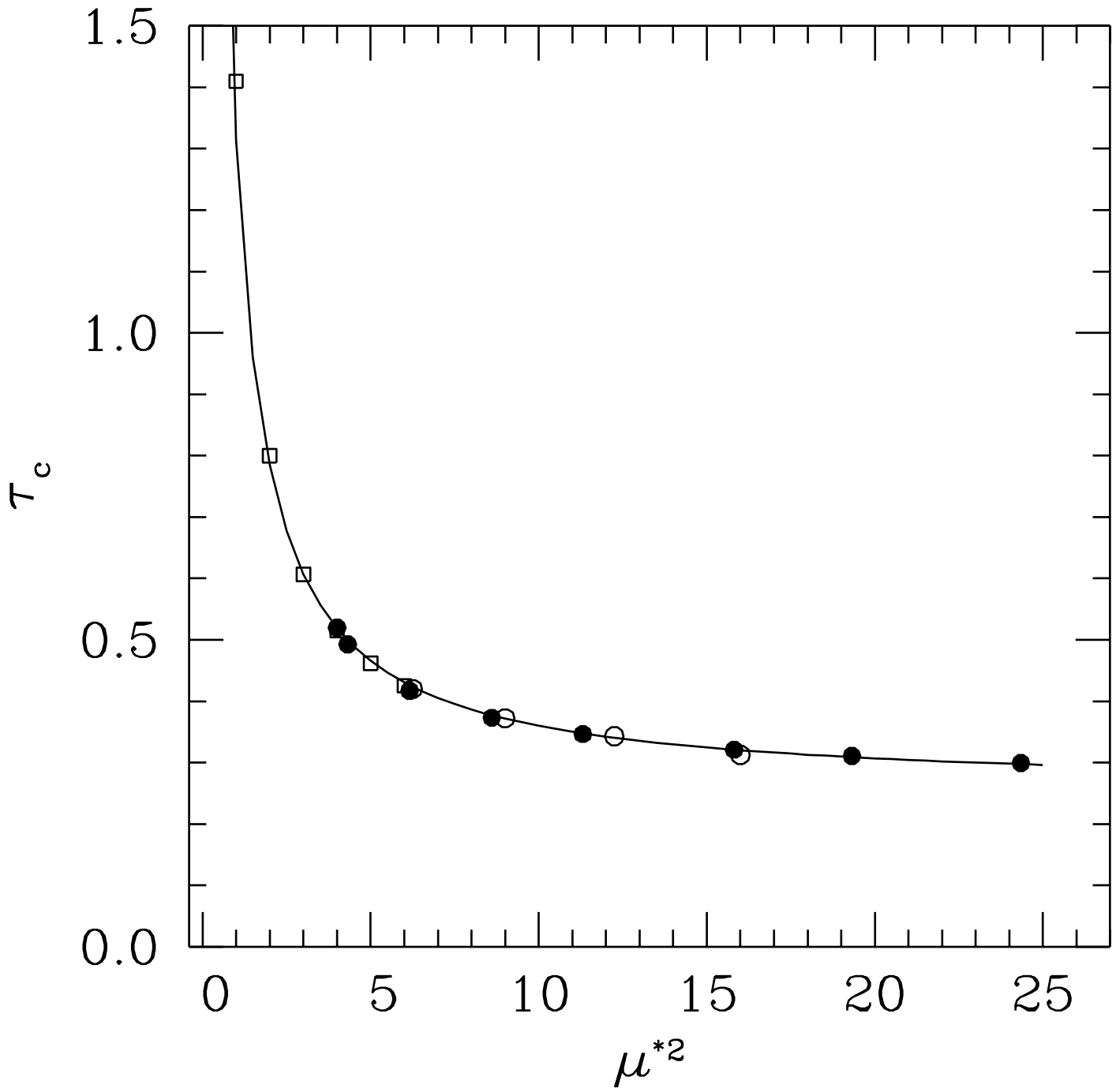

Figure 2

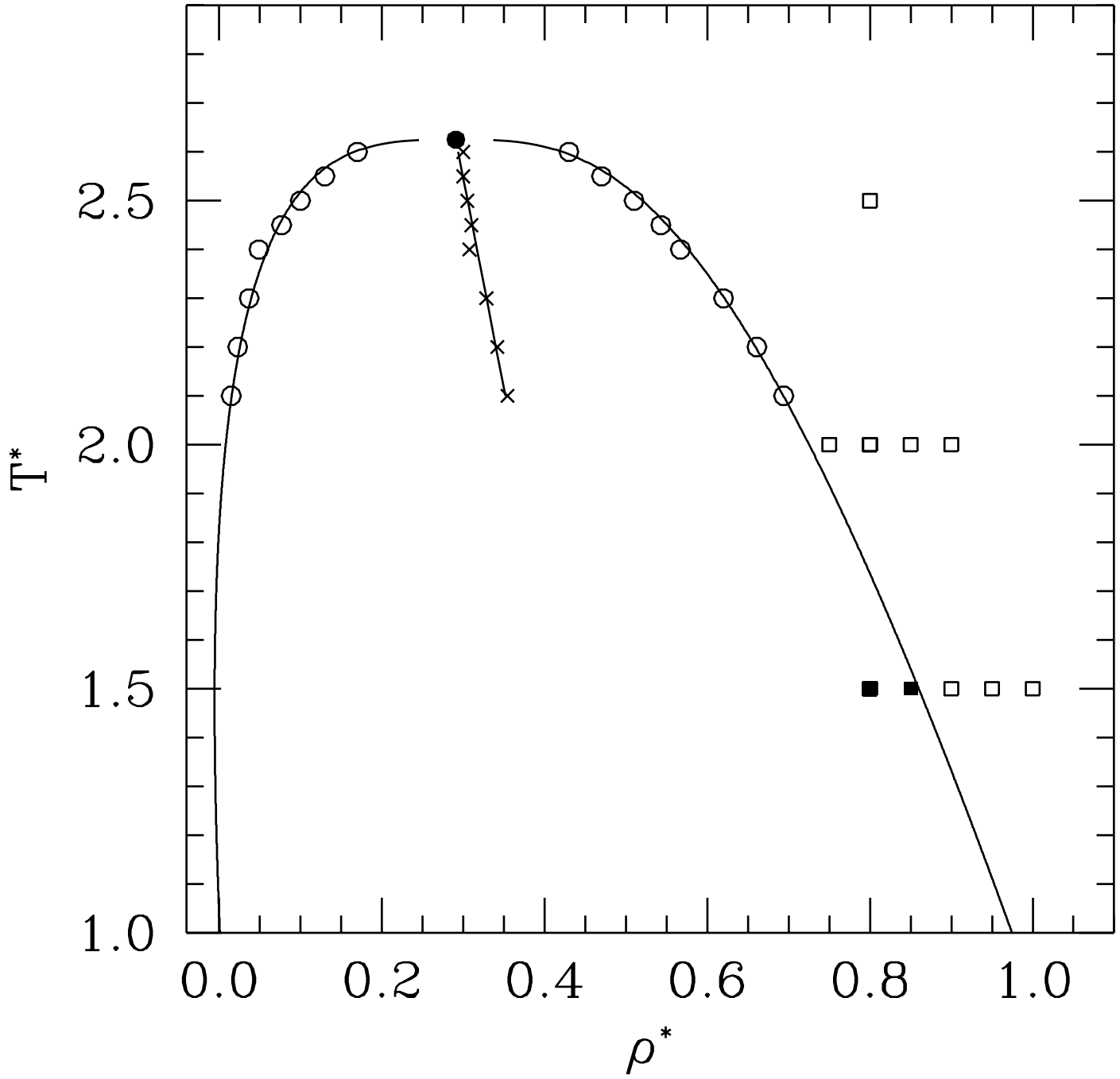

Figure 3

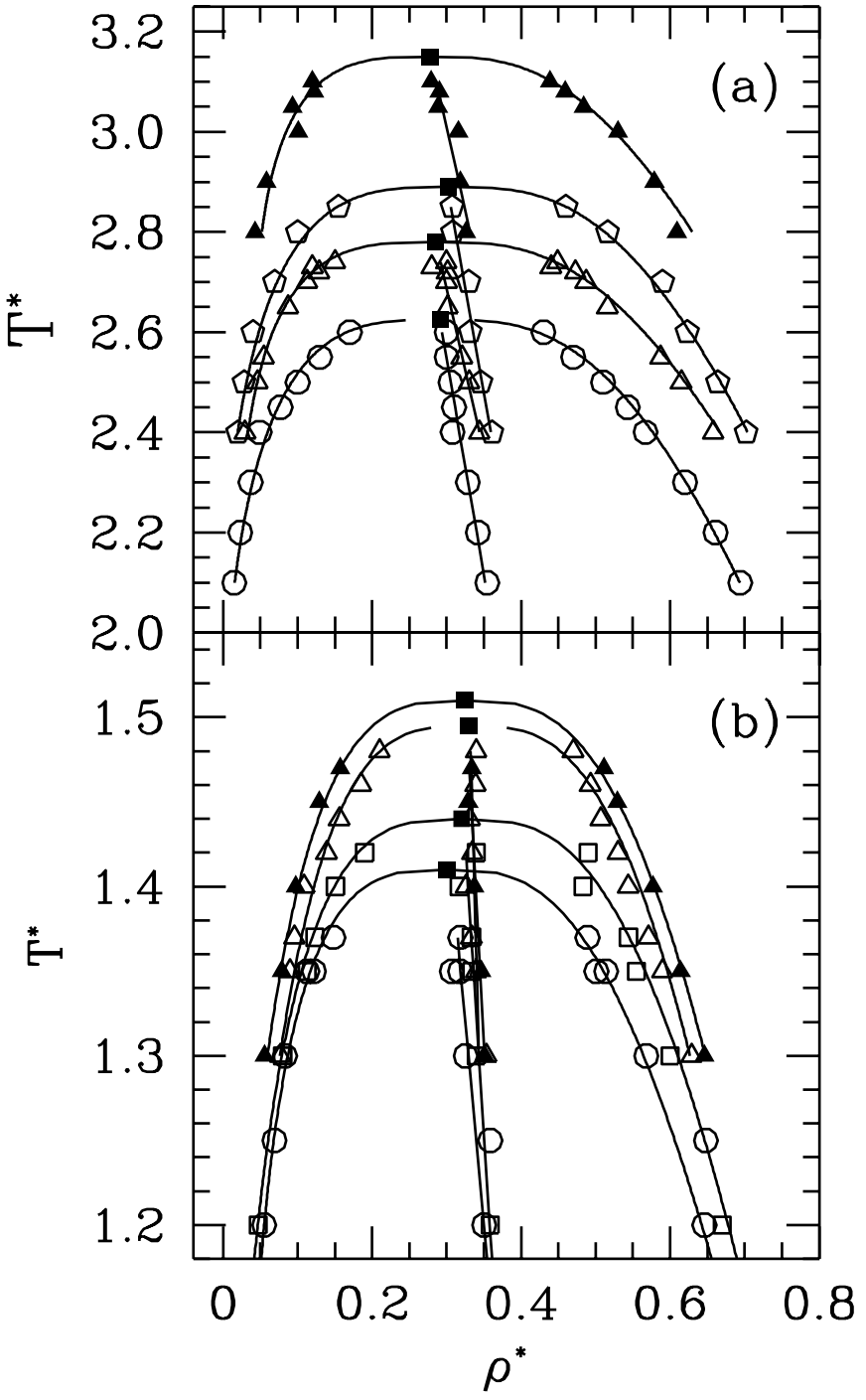

Figure 4

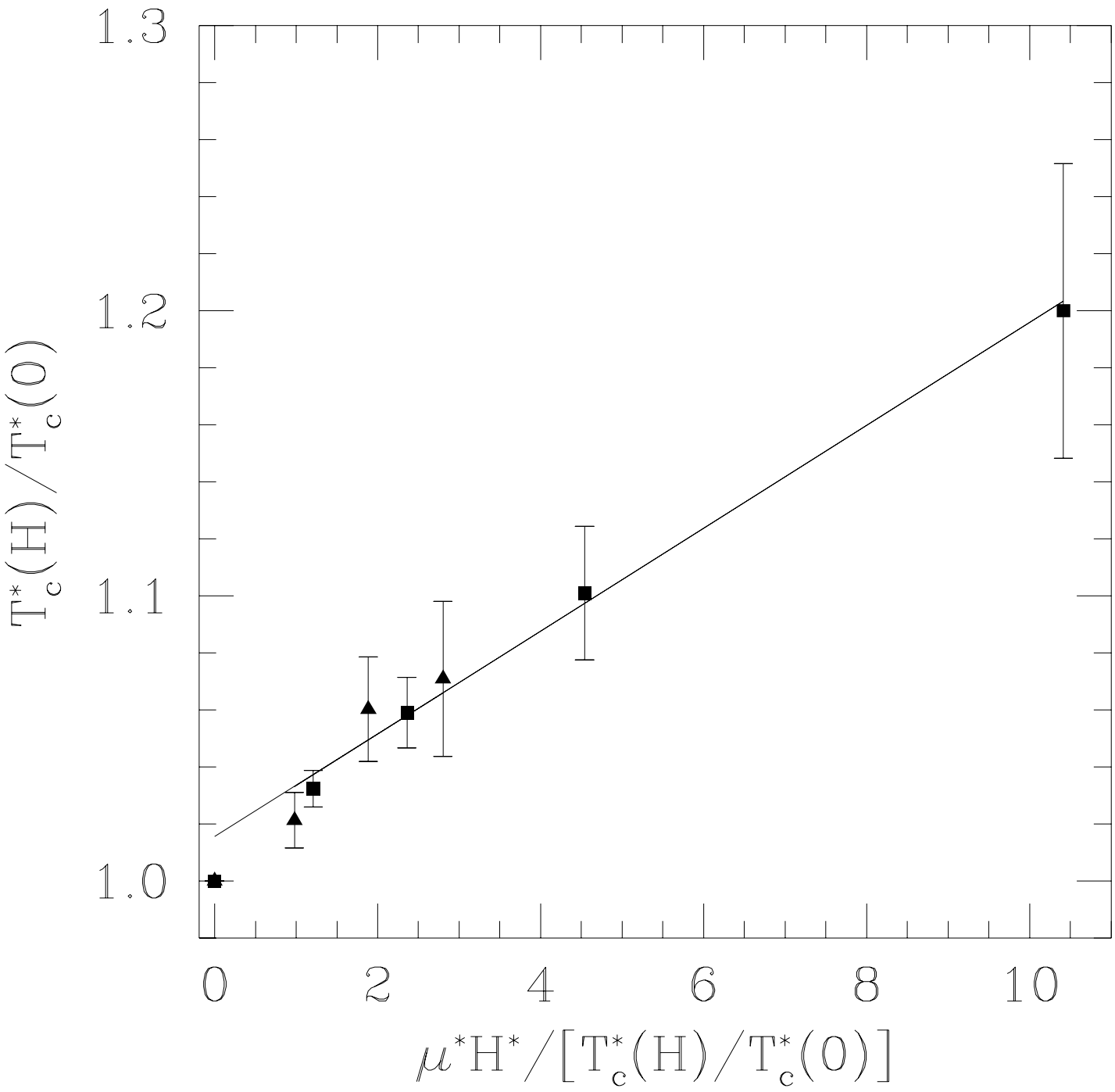

Figure 5

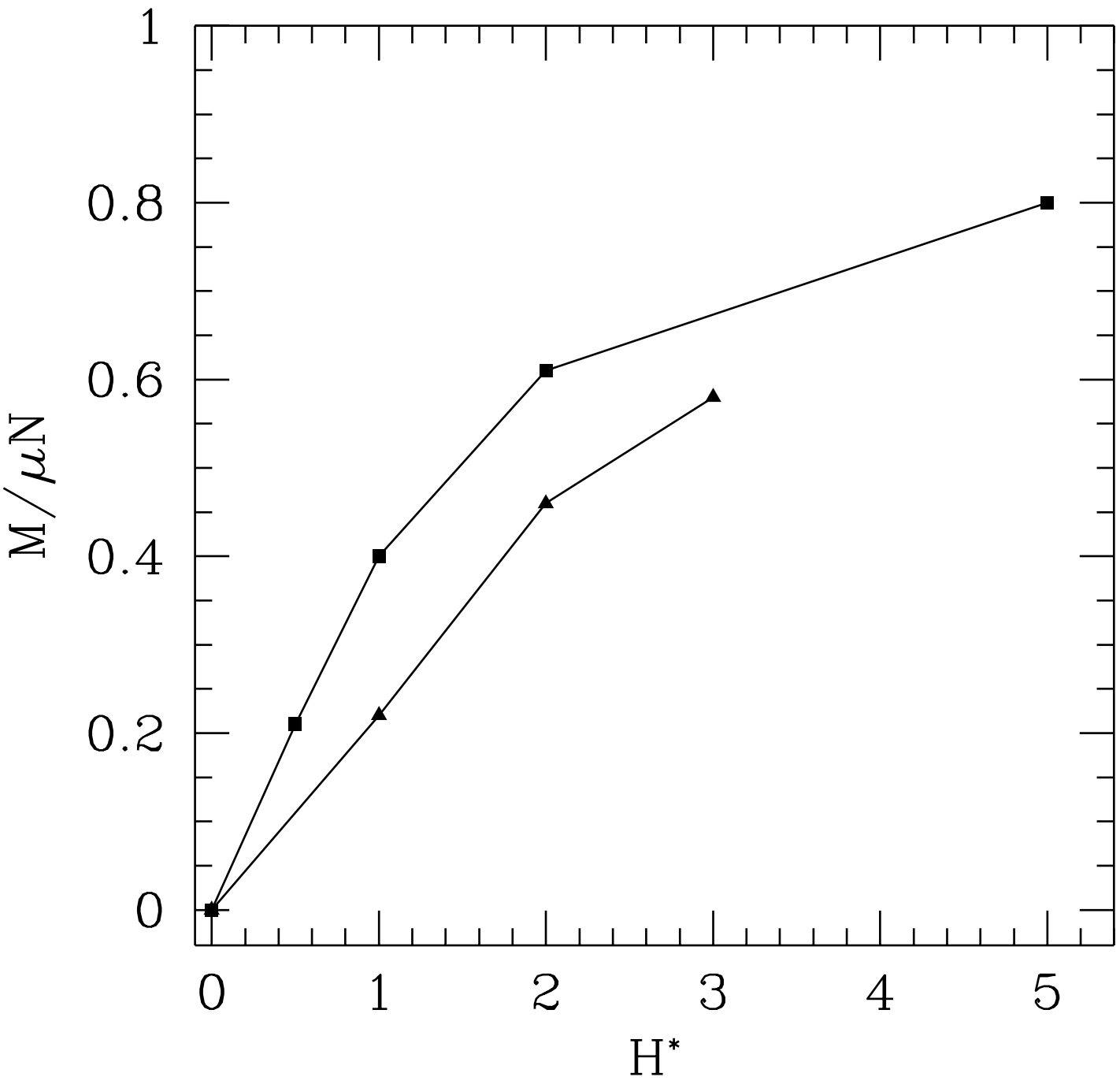

Figure 6

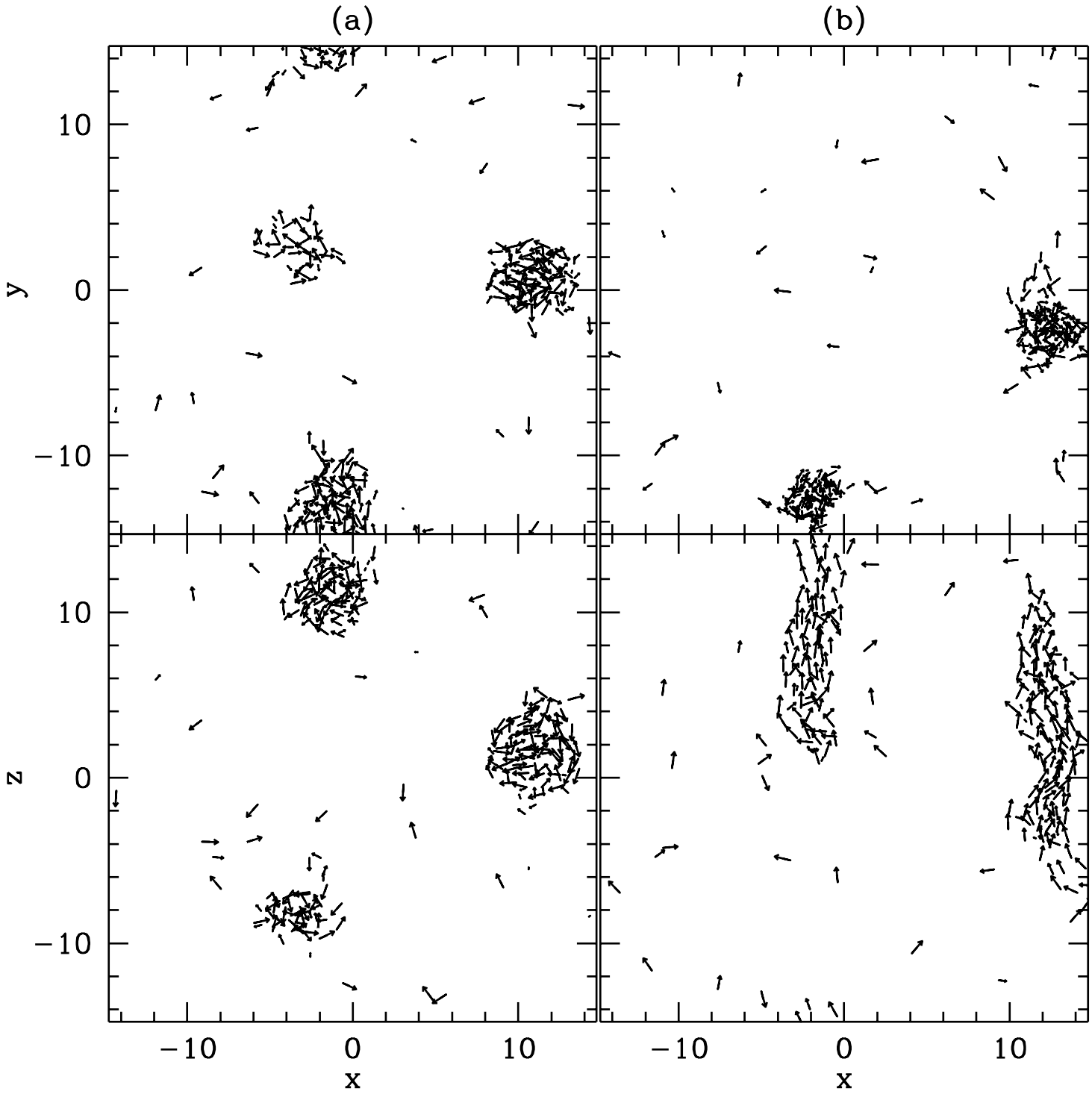

Figure 7